journal of the mechanical behavior of biomedical materials 122 (2021) 104665

Contents lists available at ScienceDirect

Journal of the Mechanical Behavior of Biomedical Materials

journal homepage: www.elsevier.com/locate/jmbbm

Research paper

A microstructural model of tendon failure

James Gregory [a,*], Andrew L. Hazel [a], Tom Shearer [a,b]

[a] Department of Mathematics, University of Manchester, Manchester, UK
[b] Department of Materials, University of Manchester, Manchester, UK

ARTICLE INFO

Keywords:
Soft tissue mechanics
Tendon
Multiscale
Microstructural
Failure

ABSTRACT

Collagen fibrils are the most important structural component of tendons. Their crimped structure and parallel arrangement within the tendon lead to a distinctive non-linear stress–strain curve when a tendon is stretched. Microstructural models can be used to relate microscale collagen fibril mechanics to macroscale tendon mechanics, allowing us to identify the mechanisms behind each feature present in the stress–strain curve. Most models in the literature focus on the elastic behaviour of the tendon, and there are few which model beyond the elastic limit without introducing phenomenological parameters. We develop a model, built upon a collagen recruitment approach, that only contains microstructural parameters. We split the stress in the fibrils into elastic and plastic parts, and assume that the fibril yield stretch and rupture stretch are each described by a distribution function, rather than being single-valued. By changing the shapes of the distributions and their regions of overlap, we can produce macroscale tendon stress–strain curves that generate the full range of features observed experimentally, including those that could not be explained using existing models. These features include second linear regions occurring after the tendon has yielded, and step-like failure behaviour present after the stress has peaked. When we compare with an existing model, we find that our model reduces the average root mean squared error from 4.53MPa to 2.29MPa, and the resulting parameter values are closer to those found experimentally. Since our model contains only parameters that have a direct physical interpretation, it can be used to predict how processes such as ageing, disease, and injury affect the mechanical behaviour of tendons, provided we can quantify the effects of these processes on the microstructure.

1. Introduction

Tendons are composed of a complex hierarchy of collagen-based components embedded within an extra-collagenous matrix. When modelling the mechanical response of tendons as they are stretched to failure, it is important to consider this complex microstructure and how it gives rise to the observed stress–strain behaviour illustrated in Fig. 1. The macroscale tendon stress–strain curve can be split into four sections: (I) the non-linear toe region, (II) the linear region, (III) the post-yield region, and (IV) the macroscopic failure region. Existing microstructural models (Hurschler et al., 1997; Hamedzadeh et al., 2018) are able to capture this behaviour when it resembles the idealised case presented in Fig. 1, but we will show that a significant proportion of observed stress–strain curves (Goh et al., 2018) contain features that cannot be explained using these models. These features include second linear regions (in region III) and step-like failure behaviour (in region IV), as shown in Fig. 2. We therefore propose a new microstructural model, based on the response of individual collagen fibrils, which is capable of capturing this behaviour.

Collagen fibrils often form the basis of microstructural models because they are the smallest component of tendons for which we have reliable stress–strain data. Fibrils are crimped within the fascicle, and only become load-bearing once the tendon has been stretched enough to remove their crimp. Due to varying crimp between fibrils, the tendon initially exhibits a non-linear stress–strain response, as fibrils gradually become taut (region I). The tendon stiffness continues to increase until all of the fibrils are taut and we see a macroscale linear region (region II). Hijazi et al. (2019) used scanning electron microscopy to show that stretching a tendon past the end of its linear region results in permanent damage on the fibril scale, suggesting that as we pass into the post-yield region (region III), fibrils themselves begin to yield. This is further supported by Zitnay et al. (2017), who were able to detect damage at the molecular level in rat tail tendon fibrils, once the tendon had been stretched past its linear region. When the tendon reaches the macroscopic failure region (region IV), many of the fibrils have yielded, and some may have ruptured completely. Eventually all of the fibrils will rupture and the tendon will fail.

* Corresponding author.
E-mail address: james.gregory@manchester.ac.uk (J. Gregory).

https://doi.org/10.1016/j.jmbbm.2021.104665
Received 8 March 2021; Received in revised form 27 May 2021; Accepted 25 June 2021
Available online 30 June 2021

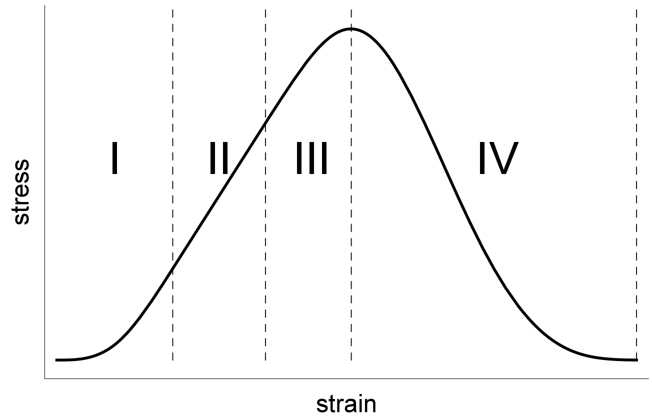

Fig. 1. Idealised stress–strain behaviour of a tendon stretched to failure. Region I is the non-linear toe region, where collagen fibrils gradually become taut, increasing the overall tendon stiffness. Region II is the linear region, where all the fibrils are exhibiting a linearly elastic response. The end of region II is the macroscopic yield point, where yielding in the fibrils causes a reduction in gradient. Region III is the post-yield region, where fibrils begin to yield and fail. Region IV is the macroscopic failure region, where fibrils continue to fail and the whole tendon eventually ruptures.

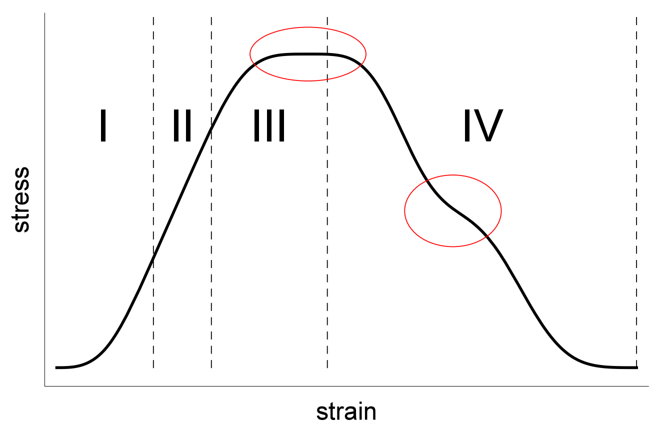

Fig. 2. An idealised stress–strain curve demonstrating observed features (highlighted in red) which cannot be captured using existing models (Hurschler et al., 1997; Hamedzadeh et al., 2018). Regions I and II are the same as in Fig. 1, but the post-yield region (region III) shows a plateau instead of a well-defined peak. The macroscopic failure region (region IV) contains step-like failure behaviour, where the second derivative of the stress changes sign multiple times.

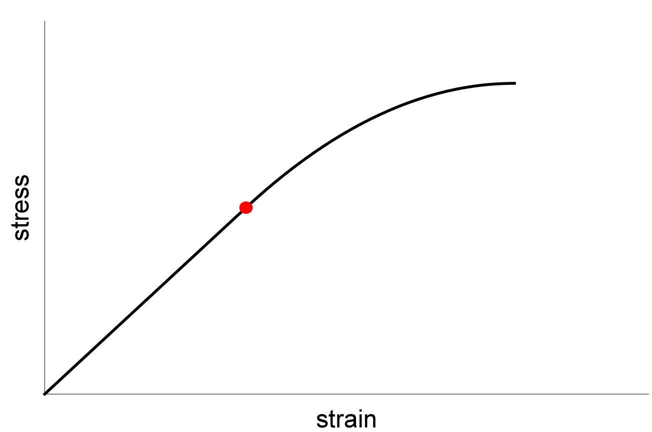

Fig. 3. Idealised stress–strain behaviour of an individual collagen fibril stretched to failure. The fibril exhibits a linear response initially, before experiencing a decrease in gradient. Stretching beyond the linear region causes the fibril to become damaged (Shen et al., 2008), leading us to refer to the transition between linear and non-linear behaviour as the fibril yield stretch/strain, represented above by the red marker.

To build a microstructural model capable of describing the full range of tendon stress–strain behaviour observed in regions I–IV, we must look in more detail at the mechanical response of individual collagen fibrils. Many research groups have performed failure tests on isolated fibrils (Shen et al., 2008, 2010; Liu et al., 2016; Yamamoto, 2017; Yamamoto and Nakamura, 2017; Svensson et al., 2013), and whilst the reported material parameters show a large amount of variability, several trends still emerge. The fibril stress–strain response is most often described as linear initially, before becoming non-linear with a decreasing slope (Shen et al., 2008, 2010; Liu et al., 2016; Yamamoto, 2017; Yamamoto and Nakamura, 2017). Van Der Rijt et al. (2006) reported non-linear toe-regions for small strains (<4%), but claim that the stress–strain curve appears to be almost perfectly linear when the fibril is stretched further. For this reason, we make the assumption that the non-linear toe-region is negligible and that the initial phase of the fibril stress is linear. Fig. 3 shows an idealised stress–strain curve for an isolated collagen fibril stretched to failure. We refer to the transition between the linear and non-linear behaviour as the fibril yield stretch/strain because there is evidence that stretching beyond this point leads to the accumulation of damage in the fibril (Shen et al., 2008). The fibril yield strain can vary considerably between fibrils extracted from different sources. It has been reported to be approximately 6% strain in groups of rabbit patellar tendon fibrils (Miyazaki and Hayashi, 1999), and 12% in single rat patellar tendon fibrils (Liu et al., 2016). In fibrils extracted from sea cucumber dermis, the yield strain shows a large amount of variation, falling anywhere between 6%–55% strain (Shen et al., 2010). After yielding and experiencing a decrease in modulus, the fibrils rupture at anywhere from 7% strain (Yamamoto and Nakamura, 2017) to over 100% strain (Shen et al., 2010). We can conclude that there is not a single value of fibril yield/rupture strain, but rather there is a distribution of these strains present in any given tendon. We also know that the structure of fibrils in tendons is not uniform. For example, the fibril diameter follows a trimodal distribution (Chang et al., 2020). It is possible that these mechanical and structural properties are related.

Ideally, a microstructural model will only contain parameters that can be measured experimentally. This allows the model to predict how certain processes, such as ageing, disease, or injury, may affect macroscale tendon behaviour, provided we know how the microstructural components are affected. For example, in the tendons of patients with classic Ehlers–Danlos syndrome (cEDS), the distribution of collagen fibril diameters is disrupted by a reduced quantity of collagen V (Sun et al., 2015), resulting in a diameter distribution with increased broadness and a larger mean diameter. A microstructural model that incorporates fibril diameter dependence could therefore be used to predict how the macroscale tendon properties would differ in comparison to a patient without cEDS. This approach would be particularly useful in instances where the effects of a disease on the mechanical properties of the tendon are not clear, as it would allow some properties, such as fibril diameter distribution, to be held constant whilst others, such as fibril density, are varied.

Continuum damage models are frequently used to predict the post-yield behaviour of tendons as they are stretched to failure, although they often contain parameters that are not based on the microstructure. Natali et al. (2003, 2005) published a model where the strain energy function of the tendon is split into two parts associated with the matrix and fibrils, with each part being premultiplied by a damage function. The fibril damage function was derived by considering the number of fibrils which had yielded, assuming that the critical stretch required to remove crimp from the fibrils is normally distributed. The strain energy function used for the elastic regime, however, was phenomenological and not related to the mechanical behaviour of individual collagen fibrils. Similar models were published by Rodríguez et al. (2006) and Alastrué et al. (2007), where the behaviour of collagen fibrils is described by models based on polymer mechanics. Whilst these models are capable of predicting the general behaviour of tendons stretched to failure, they are all phenomenological to some degree and, consequently, they contain parameters that cannot be directly measured. Other models have used a microstructural approach, but were limited to modelling regions I and II of the stress–strain curve (Shearer, 2015b,a; Shearer et al., 2020).

Extending the widely used collagen recruitment model of Lanir (1983), Hurschler et al. (1997) developed an approach to model past the end of the linear region by including a yield criterion for the fibrils. By excluding both crimped and ruptured fibrils from stress calculations, Hurschler et al. (1997) were able to get reasonable fits to data by assuming the fibril critical stretch follows a Weibull distribution. Hamedzadeh et al. (2018) independently arrived at the same model, but extended its applicability by allowing the tissue to be compressible. They also showed how to model the effects of repeated overloading, demonstrating that it is possible to predict hysteresis whilst ignoring viscoelastic effects. The models of Hurschler et al. and Hamedzadeh et al. which we shall refer to after their authors as the HLV and HGF models, respectively, show that it is possible to model whole tendon behaviour as it is stretched to failure by only focussing on the failure behaviour of the fibrils.

In this paper we use stress–strain data from Goh et al. (2018) to demonstrate the need for a new microstructural model of tendon failure. This stress–strain data was collected from failure tests carried out on mouse tail tendon fascicles, extracted from mice of different ages. The authors also provide structural data in the form of fibril diameter distributions, making it possible to explore the relationship between some of the structural and mechanical properties of tendons. In Section 2, we attempt to fit a simplified version of the HLV and HGF models to this stress–strain data, showing that a significant proportion (47%) of the data contains features that cannot be accounted for using these models.

In Section 3, we introduce a new model which is capable of capturing the range of stress–strain behaviour observed by Goh et al. (2018). By using distributions to represent the fibril yield and rupture stretches, we demonstrate the range of stress–strain behaviour that can be generated by varying the shape of the distributions, and their position relative to one another. The resulting model includes only parameters that can, in principle, be measured directly, and can fit a wider range of stress–strain data than previous models once appropriate distributions have been selected. In Section 4, we present some example fits to datasets with the features illustrated in Fig. 2. We show that the parameter values found through fitting are consistent with those found experimentally.

2. Fitting existing models to data

2.1. The elastic-rupture model

We first define the *elastic-rupture* (ER) model, which is equivalent to the HLV model (Hurschler et al., 1997). We assume that the tendon is incompressible and composed of parallel, crimped fibres embedded within an isotropic matrix. We consider a simple uniaxial stretch λ applied to the tendon, in the direction of the fibres, leading to a homogeneous stress field throughout the tissue. Each fibril has a critical stretch λ_C, which is the tendon stretch required to remove the crimp from the fibril. Once a fibril is taut, it exhibits a linear elastic response until it ruptures after being stretched by a factor of λ_R. By using a probability distribution $\Lambda_C(\lambda_C)$ to represent the variation of crimp found throughout the tissue, we can compute the stress in the tendon.

The shear modulus of the matrix has been estimated to be on the order of 1 kPa (Shearer et al., 2017), which is ∼1,000,000 times smaller than the fibril Young's modulus (Yamamoto and Nakamura, 2017). Assuming the matrix Young's modulus is of a similar magnitude, it is negligible compared to that of the fibrils, and we therefore choose to ignore any contributions to the stress from the matrix. We further assume that the deformation occurs at a strain rate that minimises hysteresis, allowing us to ignore viscoelastic effects. Under these assumptions, the stress in the tendon is given by

$$\sigma_T^{ER}(\lambda) = \phi \int_1^{\infty} \sigma_f^{ER}(\lambda, \lambda_C, \lambda_R)\Lambda_C(\lambda_C)\mathrm{d}\lambda_C. \tag{1}$$

where ϕ is the collagen volume fraction, and σ_f^{ER} is the fibril stress. In the ER model, we define the fibril stress as

$$\sigma_f^{ER}(\lambda, \lambda_C, \lambda_R) = \begin{cases} 0, & \lambda < \lambda_C, \\ E\left(\dfrac{\lambda}{\lambda_C} - 1\right), & \lambda_C \le \lambda < \lambda_C\lambda_R, \\ 0, & \lambda \ge \lambda_C\lambda_R, \end{cases} \tag{2}$$

where E is the fibril Young's modulus. For the models used in this paper, we adopt a naming approach based on the physical behaviour of the fibrils. In the ER model, the fibrils are linearly elastic until they have been stretched by a factor of λ_R, after which they rupture. Throughout this paper, we will assume that the fibril critical stretch follows a triangular distribution, as in Hamedzadeh et al. (2018), defined by

$$\Lambda_C(\lambda_C) = \begin{cases} 0, & \lambda_C < a, \\ \dfrac{2(\lambda_C - a)}{(b-a)(c-a)}, & a \le \lambda_C < c, \\ \dfrac{2(b - \lambda_C)}{(b-a)(b-c)}, & c \le \lambda_C < b, \\ 0, & \lambda_C \ge b, \end{cases} \tag{3}$$

where a is the lower limit, b is the upper limit, and c is the mode of the distribution. We choose this form for the critical stretch distribution in order to simplify calculations, and because it allows us to write down an analytic expression for the tendon stress σ_T^{ER}. This expression can be found in Appendix A. Through careful choice of the parameters a, b, and c, a triangular distribution can be used to approximate other distributions which may be more realistic for collagen fibril properties, such as a Gaussian distribution.

2.2. Fitting approaches

We now fit the ER model to stress–strain data from Goh et al. (2018). This data was gathered from mouse tail tendon fascicles, extracted from mice of different ages, which were stretched to failure. Along with stress–strain data, Goh et al. provide the tendon yield strain for each test specimen, and the mean collagen volume fraction for each age group. The authors defined the tendon yield strain to be the point with maximum gradient between the origin and the peak stress, after fitting a fifth order polynomial to the data. We explored two different fitting approaches, one which uses the yield stretch provided by Goh et al. and one which does not. In both cases we use the collagen volume fraction found by Goh et al. These two approaches are outlined below:

Generic fitting approach: Fitting for all of the model parameters: a, b, c, E, and λ_R, using the whole range of stress–strain data (regions I–IV).

Physically motivated fitting approach: We assume $a = 1$, meaning that some of the fibrils immediately become taut upon stretching the tendon. We set the fibril rupture stretch λ_R to be equal to the macroscopic yield point, provided by Goh et al. We then fit for the parameters b, c, and E using the data in regions I and II.

In both fitting approaches, we use the analytic form of the tendon stress (see Appendix A) along with a non-linear least squares method to find the fitting parameters. When using the generic fitting approach, it was often the case that the parameter values found were unphysical. For example, in Fig. 4, $b > \lambda_R$, suggesting that some fibrils begin to rupture before all of the fibrils have become taut. Whilst this seems reasonable if there is a large range of fibril critical stretch values, it contradicts evidence from Hijazi et al. (2019), that damage only occurs

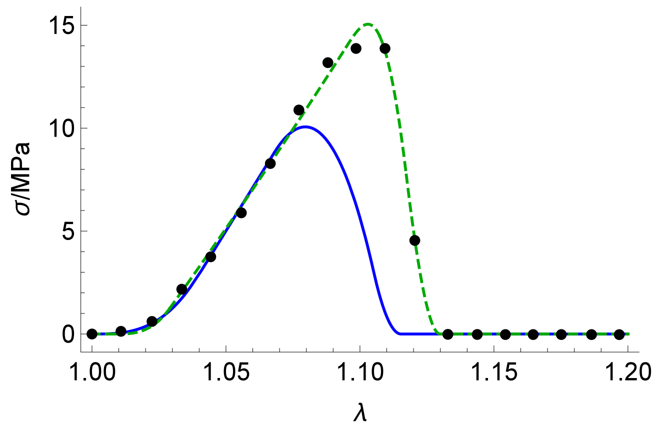

Fig. 4. The ER model fitted to data from Goh et al. (2018), using two different fitting approaches. The green dashed line was found using the generic fitting approach, whilst the solid blue line is the result of using the physically motivated fitting approach. The parameters from the generic fitting approach are: $E = 6658$ MPa, $a = 1.008$, $b = 1.107$, $c = 1.095$, and $\lambda_R = 1.020$. The parameters for the physically motivated fitting approach are: $E = 386.7$ MPa, $a = 1.0$, $b = 1.044$, $c = 1.035$, and $\lambda_R = 1.068$. The collagen volume fraction for both fittings is $\phi = 0.56$, which was taken from Goh et al. (2018). The root mean squared error for the generic approach is 0.264 MPa, whilst for the physically motivated approach it is 3.43 MPa. The generic fitting approach provides a superior fit, but at the cost of unphysical parameter values.

in the fibrils once the entire tendon has been stretched beyond the end of the macroscopic linear region (i.e. $\lambda_R \geq b$). Furthermore, the generic fitting approach often leads to unrealistically high values of collagen fibril Young's modulus E. In Fig. 4 we have $E = 6658$ MPa, which is significantly larger than the highest value we could find in any paper where isolated collagen fibrils have been stretched to failure (1900 ± 500 MPa for bovine achilles tendon fibrils under ambient conditions Grant et al., 2008).

Using the generic fitting approach requires the entire range of stress–strain data (regions I–IV), in order to determine the parameters a, b, c, E, and λ_R. If we were only interested in modelling the elastic tendon behaviour (regions I–II), the ER model could be modified by changing the fibril stress, defined in Eq. (2), so that the fibrils never rupture ($\lambda_R = \infty$). Since this elastic version of the model is defined by the same set of parameters, excluding λ_R, we should be able to determine the elastic parameters (a, b, c, and E) with the data from regions I and II alone. In other words, we should not need to stretch a tendon to failure in order to determine the parameters that define the pre-yield portion of the stress–strain curve. The physically motivated fitting approach ensures that $\lambda_R \geq b$, and that the elastic parameters are determined using the elastic part of the stress–strain data alone. Fig. 4 shows an example of these two fitting approaches on the same set of data.

The restrictions placed on the model's parameters when using the physically motivated fitting approach mean that in the vast majority of cases, it is not possible to get a good fit to the data in regions III and IV. The magnitude of the post-yield stress is consistently underestimated, as can be seen in Fig. 4, suggesting that there is something missing from the model. Although the ER model can provide a reasonable fit in certain cases when the generic fitting approach is used, we instead choose to modify the model so that we can still use the physically motivated fitting approach. This ensures that all fitting parameters are realistic, and that the elastic parameters are consistent with the values we would find if the tendon was not stretched to failure.

2.3. Features that cannot be accounted for

The ER model is only capable of describing the mechanical response of tendons in the cases where the stress–strain curve looks similar to the idealised response illustrated in Fig. 1. In the stress–strain data from Goh et al. (2018), a significant proportion of the data contains features that cannot be captured using the ER model, even when the constitutive behaviour of the fibrils is adjusted to more closely resemble experimental data. In this section we describe these features, discuss their prevalence, and demonstrate why a new model is required to capture them. A summary of the information presented in this section, split according to the age of the mouse from which the fascicle was extracted, can be seen in Table B.1 of Appendix B.

2.3.1. Additional linear regions

The idealised stress–strain curve in Fig. 1 contains one linear region, in the elastic part of the response. Some sets of stress–strain data from Goh et al. (2018) also contain a second linear region, present after the tendon has yielded. The gradient of this second linear section can vary, but is always less than the gradient of the first linear section. In some cases we see a small decrease in gradient as the tendon yields and enters a second linear region, followed by a well-defined peak in the stress. In other cases, the gradient of the second linear region is close to zero, and the stress reaches a plateau rather than a well-defined peak.

To determine whether a stress–strain curve contains a second linear region, we first isolate the data points before the peak. We then interpolate the data using splines over 50 equally spaced points, and look for groups of at least 10 interpolated data points where the gradient does not vary by over 10% of the maximum global gradient. Using this approach we find that 86 of 260 sets of data (~33%) contain a second linear region.

Our analysis showed that the peak can vary dramatically in broadness. Data with well-defined peaks can often be fitted using the ER model, but when the peak is wider, the ER model fails to capture the post-yield behaviour. This may be due to the fact that the ER model does not incorporate fibril plasticity, leading to an underestimation in the magnitude of the post-yield stresses at the tendon scale. The failings of the ER model are most apparent in the 33% of cases where there is a clear second linear region. Without adding fibril plasticity to the ER model, we cannot possibly achieve a plateau in the macroscale stress–strain curve.

2.3.2. Step-like failure behaviour

The second feature that cannot be accounted for using the ER model is step-like failure behaviour in the macroscopic failure region. In the idealised stress–strain curve presented in Fig. 1, the gradient of the stress in region IV begins at zero, decreasing smoothly until it reaches a minimum value, before increasing back to zero. This behaviour can be described using the ER model. In the experimental data from Goh et al. (2018), some of the stress–strain curves seem to show steps in this region, where the second derivative of the stress changes sign multiple times.

We classify a set of data as exhibiting step-like failure behaviour if there is at least one data point in region IV with a larger gradient than both of its neighbouring points. Using this criterion, we find that 54 of 260 sets of data (~21%) contain step-like failure behaviour. This is a significant proportion of the data, further supporting the need for an improved model.

3. The elastic–plastic-distribution model

3.1. General framework

By making biologically-motivated adjustments to the ER model, we can begin to account for the stress–strain features described in Section 2.3. The first of these is to modify the constitutive behaviour of the fibrils so that once they have been stretched by a factor of λ_Y, they yield and begin to undergo plastic deformation. The second is to introduce distributions for the fibril yield stretch λ_Y, and rupture stretch λ_R. We call the resulting model the *elastic–plastic-distribution* (EPD) model. In the EPD model, we define the fibril stress to be

$$\sigma_f^{EPD}(\lambda, \lambda_C, \lambda_Y, \lambda_R) = \begin{cases} 0, & \lambda < \lambda_C, \\ E\left(\dfrac{\lambda}{\lambda_C} - 1\right), & \lambda_C \leq \lambda < \lambda_C\lambda_Y, \\ p(\lambda, \lambda_C, \lambda_Y, \lambda_R), & \lambda_C\lambda_Y \leq \lambda < \lambda_c\lambda_R, \\ 0, & \lambda \geq \lambda_C\lambda_R, \end{cases} \tag{4}$$

where $p(\lambda, \lambda_C, \lambda_Y, \lambda_R)$ is the plastic stress in a yielded fibril. Experimental evidence suggests that, when selecting a functional form for p, we should choose a "flat" function which has a lower gradient than the initial linear portion of the fibril stress. We believe that in instances where the macroscale tendon stress is displaying a broad/flattened peak, the majority of fibrils are also exhibiting flattened stress–strain behaviour.

We assume that the fibril critical stretch λ_C, yield stretch λ_Y, and rupture stretch λ_R, follow a multivariate distribution $\Lambda(\lambda_C, \lambda_Y, \lambda_R)$. We then find the stress in the tendon by integrating the fibril stress over this distribution,

$$\sigma_T^{EPD}(\lambda) = \phi \int_1^\infty \int_1^\infty \int_1^\infty \sigma_f^{EPD}(\lambda, \lambda_C, \lambda_Y, \lambda_R)\Lambda(\lambda_C, \lambda_Y, \lambda_R)\mathrm{d}\lambda_C \mathrm{d}\lambda_Y \mathrm{d}\lambda_R. \tag{5}$$

3.2. Simplifying assumptions

In order to demonstrate how the EPD model can be used to produce the range of macroscale stress–strain curves observed experimentally, we make two simplifying assumptions. Firstly, we assume that the fibrils are bilinear elasto-plastic, choosing the following form for p,

$$p(\lambda, \lambda_C, \lambda_Y, \lambda_R) = E(1-k)(\lambda_Y - 1) + Ek\left(\frac{\lambda}{\lambda_C} - 1\right), \tag{6}$$

where $k \in [0, 1]$ is a factor describing the decrease in gradient after the fibril has yielded. Secondly, we assume that the critical, yield, and rupture stretches are independent of each other, so that the distribution $\Lambda(\lambda_C, \lambda_Y, \lambda_R)$ can be written as

$$\Lambda(\lambda_C, \lambda_Y, \lambda_R) = \Lambda_C(\lambda_C)\Lambda_Y(\lambda_Y)\Lambda_R(\lambda_R). \tag{7}$$

We further assume that $\Lambda_C(\lambda_C)$, $\Lambda_Y(\lambda_Y)$, and $\Lambda_R(\lambda_R)$ are all triangular distributions. By changing the values of the parameters defining the yield and rupture stretch distributions, we can control the width of the macroscale stress–strain curve in regions III and IV. This amount of control is not possible using the ER model, and is required in order to fit the range of data observed experimentally.

3.3. Marginal distributions

In the HGF model (Hamedzadeh et al., 2018), the authors define a damage distribution by stretching the critical stretch distribution by a factor of λ_R, their single value of rupture stretch. This damage distribution describes the proportion of fibrils in the tendon that have failed for a given value of tendon stretch. We can also compute equivalent distributions for the yield and rupture stretch when we have distributions, rather than single values.

A fibril with critical stretch λ_C, and yield stretch λ_Y, will yield when the tendon stretch is equal to $\lambda = \lambda_C\lambda_Y$. We consider the joint distribution of critical stretch and yield stretch, and use this relation to define the following function

$$g(\lambda_C, \lambda) = \Lambda_C(\lambda_C)\Lambda_Y\left(\frac{\lambda}{\lambda_C}\right). \tag{8}$$

We then define $\overline{\Lambda_Y}(\lambda)$ as the marginal distribution found by integrating $g(\lambda_C, \lambda)$ with respect to λ_C,

$$\overline{\Lambda_Y}(\lambda) = \int_1^\infty g(\lambda_C, \lambda)\mathrm{d}\lambda_C = \int_1^\infty \lambda_C(\lambda_C)\Lambda_Y\left(\frac{\lambda}{\lambda_C}\right)\mathrm{d}\lambda_C. \tag{9}$$

We can follow a similar process in order to determine the marginal rupture distribution $\overline{\Lambda_R}(\lambda)$. The resulting distributions, once normalised, can be used to describe the proportion of fibrils that have yielded or ruptured for a given tendon stretch λ. Hamedzadeh et al. (2018) show the tendon stress–strain curve obtained using their model when the damage distribution (marginal rupture distribution in our model) and critical stretch distribution overlap. If these distributions overlap, then the first fibril may fail before the last fibril becomes taut, a scenario we argued against when justifying the physically motivated fitting approach. It is possible, however, that the marginal *yield* distribution and the marginal rupture distribution can overlap in our model. As discussed in Section 1, there is a large range of yield and rupture strain values reported in the literature, even for fibrils extracted from the same source. It is therefore possible that as a tendon is stretched to failure, some fibrils rupture before others have yielded.

3.4. Varying the stretch distributions

By varying the shape, position, and spread of the yield stretch and rupture stretch distributions, it is possible to produce macroscale stress–strain curves with the full range of features observed experimentally. Fig. 5 shows the effects of varying the separation between the distributions, with all other parameters fixed. To produce this figure we used generic parameter values, varying only the mean rupture stretch, to demonstrate the effects this has on the macroscale tendon stress. Based on the limited data in the literature, any of these arrangements could be possible, and we provide a more detailed discussion about the possible values of the distribution parameters in Section 5.

When the distributions overlap, there is a well-defined peak with no second linear region. Increasing the separation between the yield and rupture distributions causes a plateau to appear in the macroscale stress–strain curve, for values of tendon stretch between the marginal distributions. In this region, when there is no overlap, all of the fibrils are deforming plastically. By choosing the constitutive behaviour of the fibrils to be bilinear elasto-plastic, this leads to a second linear region. The spread of the yield and rupture distributions also affects the macroscale stress–strain curve, as can be seen in Figs. 6 and 7.

In Fig. 6 we see that changing the spread of the rupture distribution, whilst holding the yield distribution constant, changes the shape of the peak and increases the width of region IV. As the spread increases, there is more overlap, and the peak becomes sharper. This is due to the fibrils rupturing sooner, and therefore no longer contributing to the macroscale stress. Fig. 5 shows how translating the rupture stretch distribution to the right can result in a significant increase to the magnitude of the post-yield stress. Varying the spread of the rupture distribution, however, changes the shape of the peak without causing a significant increase in the magnitude of the stress in region III.

The results displayed in Fig. 7 demonstrate how the macroscale stress–strain curve is affected when the rupture distribution is fixed and the spread of the yield distribution is varied. In doing this we choose to fix the lower bound of the yield distribution so that the macroscale yield point remains the same. By increasing the spread in the yield distribution, we are delaying the yielding of fibrils, causing an increase in the magnitude of the post-yield stress. We also increase the amount of overlap between the marginal distributions, leading to a sharper peak. The stress in the macroscopic failure region (region IV) is not affected by these changes.

The distributions used to generate the stress–strain curves in Figs. 5, 6, and 7 have all been unimodal triangular distributions. Allowing the rupture distribution to be multimodal causes the stress in the macroscopic failure region to exhibit step-like behaviour, as shown in Fig. 8. Whilst there is no direct evidence that collagen fibril failure strain follows a multimodal distribution, we consider this case because it is a simple way to introduce step-like failure behaviour on the macroscale. See Section 5 for a full discussion on alternative ways to account for step-like failure behaviour.

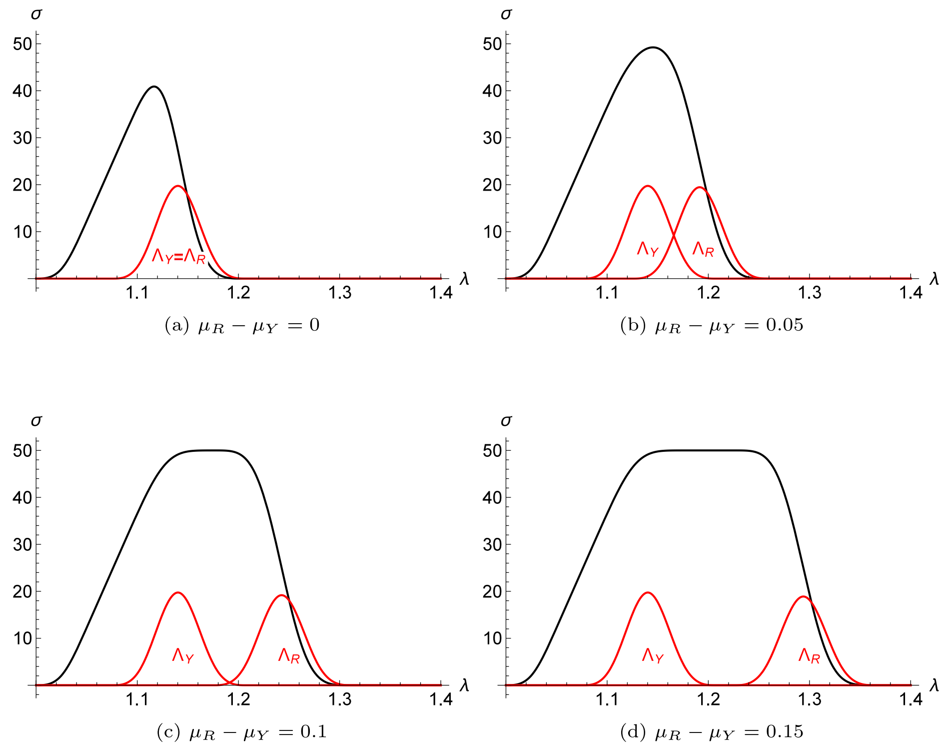

Fig. 5. The effects of varying the separation between the yield stretch and rupture stretch distributions, on the macroscale stress–strain curve. The yield distribution was fixed and the position of the rupture distribution was varied. Symmetric triangular distributions were used for all of the stretch distributions. The black curves show the stress in the tendon, whilst the red curves show the marginal yield and rupture distributions used to generate them. The mean value of the (original, not marginal) yield and rupture distributions are μ_Y and μ_R, respectively. μ_Y remains fixed at $\mu_Y = 1.1125$. We choose a value of $k = 0$ to illustrate how varying the separation between the two distributions can lead to a plateau in the tendon stress.

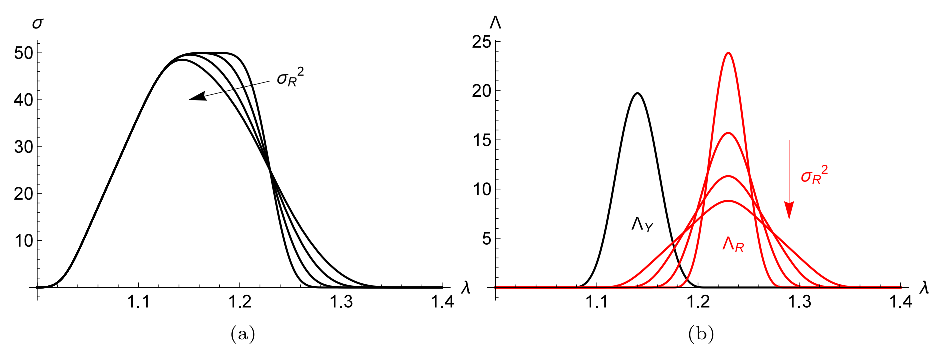

Fig. 6. When the mean values of the yield and rupture distributions are held constant and the variance of the rupture distribution is increased, the macroscale stress strain-curve changes as shown in (a). The corresponding marginal distributions are shown in (b). The arrows point in the direction of increasing variance, σ_R^2.

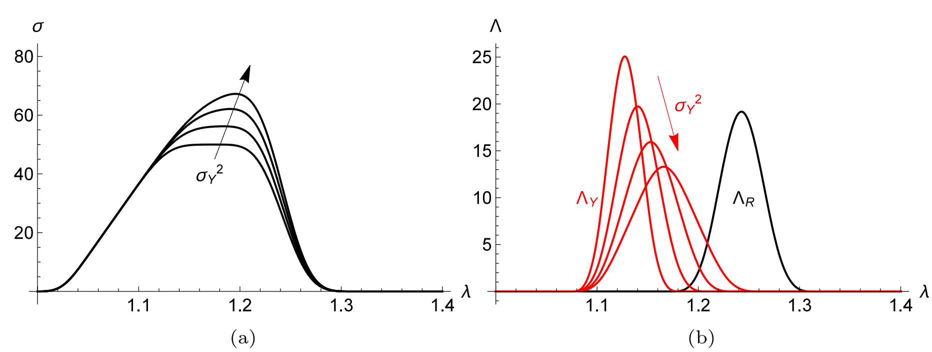

Fig. 7. Shown in (a) is the macroscale stress–strain curve obtained when the rupture stretch distribution is held constant and the variance of the yield stretch distribution is changed. The marginal distributions that generate these curves can be seen in (b). The variance is changed by increasing the upper limit of the distribution, whilst holding the lower limit constant. This is done so that the macroscale yield point remains constant in all of the stress–strain curves in (a). The arrows point in the direction of increasing variance, σ_Y^2.

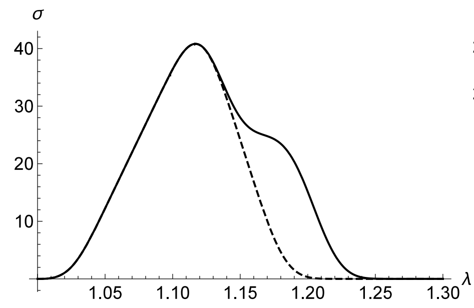

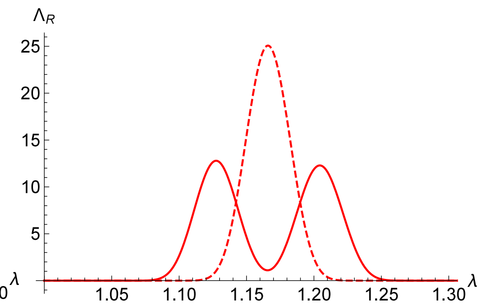

Fig. 8. Changing the fibril rupture distribution from unimodal to bimodal causes the stress in the macroscopic failure region to exhibit step-like behaviour. Shown in (a) is the macroscopic stress–strain curve generated from the rupture distributions whose marginal counterparts are shown in (b). Dashed and solid lines correspond to the unimodal distribution and bimodal distribution, respectively. In the bimodal case, fewer fibrils are rupturing when the tissue stretch λ falls between the modes, leading to a region in the macroscale stress–strain curve where the gradient becomes less steep.

When the rupture distribution used to generate the macroscale stress–strain curve is multimodal and has a sufficiently wide gap between the peaks, we see a corresponding region of the stress–strain curve where the gradient of the stress becomes less steep. As the tendon stretch approaches the next peak, the gradient of the stress becomes more negative again as fibrils continue to fail and no longer contribute to the total stress. This leads to step-like behaviour, as shown in Fig. 8a.

4. Fitting the improved model to data

In this section we use the physically motivated fitting approach to show that the EPD model can be used to generate realistic stress–strain curves, with microstructural parameters that fall within the range of values observed experimentally.

We continue to use the stress–strain data from Goh et al. (2018), using the following process to find appropriate parameter values:

1. We assume the fibril critical stretch λ_C follows a triangular distribution, defined by the parameters a, b, and c, as described in Eq. (3).
2. We use the method outlined in Section 2 to determine the elastic parameters and use the macroscopic yield point provided by Goh et al. (2018) to separate the data into elastic and inelastic parts. To reduce the number of fitting parameters we assume that the critical stretch distribution is symmetric so that $c = (a + b)/2$.
3. We assume that both the fibril yield stretch λ_Y, and fibril rupture stretch λ_R, follow symmetric triangular distributions, given by Λ_Y and Λ_R, respectively. There is not enough data available to make an informed decision about the forms of either of these distributions. Triangular distributions are used to simplify calculations and to ensure that Λ_Y and Λ_R have finite support. Additionally, a symmetric triangular distribution can be defined using just the range of observed values, making the resulting fitting parameters easy to compare with the limited data available in the literature.
4. We label the yield stretch distribution parameters as a_Y and b_Y, and the rupture stretch distribution parameters as a_R and b_R.
5. We then use a nonlinear least squares method (`scipy.optimize.curve_fit` in Python 3) to determine the five remaining parameters: a_Y, b_Y, a_R, b_R, and k.
6. If the algorithm described in Section 2.3.2 detects step-like failure behaviour, we replace the rupture stretch distribution with a bimodal triangular distribution, defined by

$$\Lambda_R^{\text{bimodal}}(\lambda_R) = \frac{1}{1+W}\left(\Lambda_R^{(1)}(\lambda_R) + W\Lambda_R^{(2)}(\lambda_R)\right), \tag{10}$$

where $\Lambda_R^{(1)}$ and $\Lambda_R^{(2)}$ are unimodal triangular distributions, as defined in Eq. (3), with distribution parameters $(a_R^{(1)}, b_R^{(1)}, c_R^{(1)})$ and $(a_R^{(2)}, b_R^{(2)}, c_R^{(2)})$, respectively. The relative weighting between the two modes is given by W. In these instances we assume $\Lambda_R^{(1)}$ and $\Lambda_R^{(2)}$ are both symmetric and fit for $a_R^{(1)}$, $b_R^{(1)}$, $a_R^{(2)}$, $b_R^{(2)}$, and W.

We also fitted the ER model to the same data, assuming that the fibril critical stretch followed a symmetric triangular distribution to ensure a fair comparison. We adopted the generic fitting approach for the ER model to get the best fit possible, but in many cases this still provided a poor fit because the ER model cannot generate plateaus or step-like failure behaviour. Of the 262 sets of stress–strain data from Goh et al., we excluded 39 (15%) because they contained fewer data points than fitting parameters. The remaining fits had an average root mean squared error (RMSE) of 2.29 MPa compared to 4.53 MPa for the ER model. Using the EPD model reduced the RMSE in 183 of the non-excluded cases (82%). In instances where step-like failure behaviour was detected, changing from a unimodal to a bimodal rupture stretch distribution reduced the average RMSE of those tests from 2.19 MPa to 1.50 MPa. Histograms of the fitting parameters can be seen in Appendix C. When defining the physically motivated fitting approach in Section 2.2, we state that the macroscopic yield point should correspond to the point at which the first fibril yields. In the EPD model this is equivalent to setting a_Y equal to the macroscopic yield point. Whilst this can provide a good fit in some cases, we opted to remove this restriction when fitting both models to the whole set of data, because in some cases it is too restrictive. This could be an indication that some fibrils begin to yield before others have become taut, or that the yield point determined by Goh et al. is inaccurate.

Fig. 9 shows an example of the EPD model fitted to data from Goh et al. (2018), containing a plateau region rather than a well-defined peak. We can achieve a good fit to this data by assuming the yield stretch and rupture stretch follow symmetric triangular distributions. The RMSE for the fit is 1.13 MPa, compared with 7.39 MPa for the ER model using the generic fitting approach. The error is considerably larger for the ER model because it cannot generate a second linear region. The initial non-linear toe region covers the support of the critical stretch distribution and the region between the supports of the critical stretch and marginal yield distributions corresponds to the macroscale linear region. Fibrils begin to yield when the tendon stretch falls within the support of the marginal yield distribution, leading to a decrease in the gradient of the stress. There is then a region before fibrils start failing, where all fibrils are deforming plastically. The stress then decreases to zero as fibrils begin to rupture.

Fig. 10 shows a second set of data from Goh et al. (2018), containing a well-defined peak along with step-like failure behaviour in region IV. The same fitting procedure was followed, but using a bimodal triangular distribution for the rupture stretch, in order to capture the step-like failure behaviour in region IV. The root mean squared error for the fit in Fig. 10 is 2.21 MPa, compared with 7.57 MPa for the ER model using the generic fitting approach. The resulting yield and

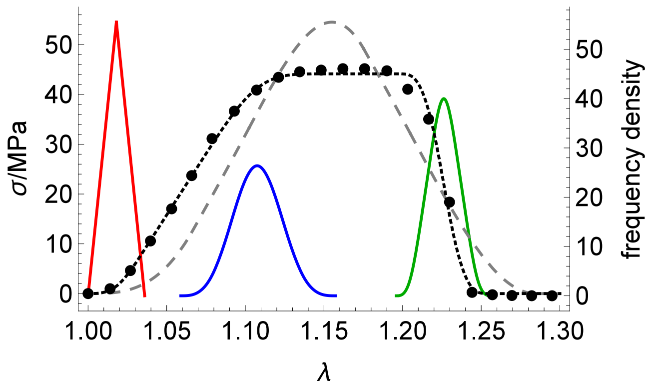

Fig. 9. The black dashed line shows the EPD model, with bilinear elastoplastic fibrils, fitted to data from Goh et al. (2018). The critical stretch distribution, shown in red, was found by fitting the purely elastic model to the data in regions I and II. The blue and green curves show the marginal yield and rupture distributions, defined in Eq. (9). The right hand axis refers to these distributions. The critical, yield, and rupture stretch were assumed to follow symmetric triangular distributions. The macroscale stress–strain curve contains a plateau region which could not be accounted for using previous models. The crimp distribution parameters are $a = 1.0$ and $b = 1.036$. The fibril Young's modulus is $E = 895.7$ MPa, and $k = 0$. The yield stretch distribution parameters are $a_Y = 1.059$ and $b_Y = 1.117$. The rupture stretch distribution parameters are $a_R = 1.196$ and $b_R = 1.213$. The RMSE for the fit is 1.13 MPa. The grey dashed line shows the ER model fitted to the same data, where the RMSE is 7.39 MPa.

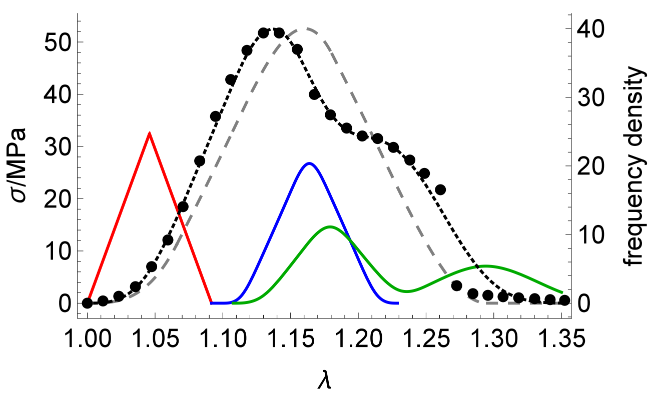

Fig. 10. The EPD model fitted to data from Goh et al. (2018) containing a well-defined peak and step-like failure behaviour. The black dashed line shows the stress, whilst the red, blue, and green curves show the critical stretch, the marginal yield stretch, and the marginal rupture stretch distributions, respectively. A bimodal rupture distribution is able to capture the step-like failure behaviour observed at the tendon level. The crimp distribution parameters are $a = 1.0$ and $b = 1.081$. The fibril Young's modulus is $E = 1160$ MPa, and $k = 0.349$. The yield stretch distribution parameters are $a_Y = 1.088$ and $b_Y = 1.112$. The rupture stretch distribution parameters are $a_R^{(1)} = 1.095$, $b_R^{(1)} = 1.131$, $a_R^{(2)} = 1.159$, and $b_R^{(2)} = 1.263$. The second peak of the rupture stretch distribution has a weighting of $W = 0.72$ relative to the first peak. The RMSE for the fit is 2.21 MPa. The grey dashed line shows the ER model fitted to the same data, with a RMSE of 7.57 MPa.

rupture stretch distributions overlap, leading to a well-defined peak in the stress. This also means that there is a range of tendon stretch values λ, where there simultaneously exists undamaged, yielded, and ruptured fibrils. The stress in the tendon begins to decrease as fibrils rupture, and once the tendon stretch passes into the region between the rupture distribution peaks, the gradient of the stress becomes less negative, because fewer fibrils are rupturing. As λ passes into the second rupture distribution peak, the gradient becomes more negative, and the tendon eventually fails.

Although the EPD model presents a good fit in the majority of cases, it can sometimes fail to capture the observed behaviour. Figs. 11 and 12 show two examples where this is the case.

The EPD model fails to capture the multiple steps present in the stress–strain data shown in Fig. 11. These could be captured by using a

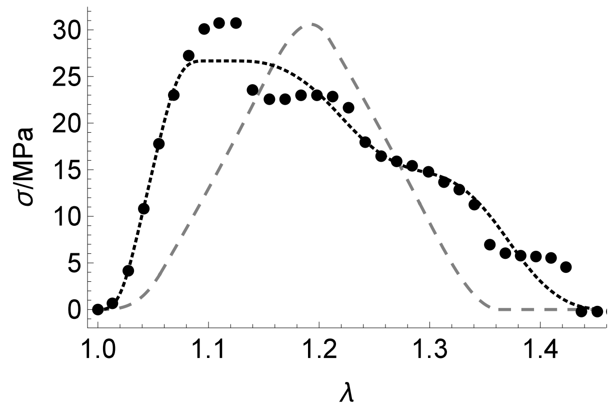

Fig. 11. The black dashed line shows the EPD model, with a bimodal rupture stretch distribution, fitted to data from Goh et al. (2018) (RMSE = 2.02 MPa). The data contains more than one step in the macroscopic failure region and so it would require more than two modes in the rupture stretch distribution to capture this behaviour. The grey dashed line shows the ER model fitted to the same data (RMSE = 8.51 MPa).

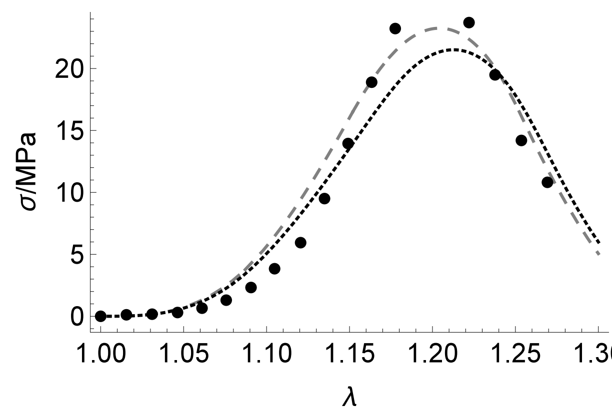

Fig. 12. The black dashed line shows the EPD model fitted to data from Goh et al. (2018) (RMSE = 2.45 MPa). Assuming that the critical stretch distribution is symmetric leads to a poor overall fit. The grey dashed line shows the ER model fitted to the same data (RMSE = 1.84 MPa).

rupture stretch distribution with more than two modes, but due to the low number of data points we chose not to attempt this. In Fig. 12, the assumption that the critical stretch distribution is symmetric leads to a poor fit in regions I and II, causing the peak stress to be underestimated.

5. Discussion

We have shown that we can construct a mathematical model of tendon failure by splitting the fibril stress into elastic and plastic parts, and allowing the fibril yield stretch and rupture stretches to follow distributions, rather than being single-valued. When a single value of these parameters is used, as in the ER model, the plastic behaviour of the tendon is determined entirely by the critical stretch distribution. In at least 47% of cases (see Appendix B) it is not possible to get a good fit using the ER model because the stress–strain data contains a second linear region, step-like failure behaviour, or both. The EPD model provides a microstructural explanation for these features, and has the additional benefit of only including parameters that can be measured directly.

The introduction of a plastic stress function to the fibril constitutive behaviour is not new. Hamedzadeh et al. (2018) define their model in terms of a general fibril constitutive behaviour, thereby encompassing that part of the EPD model. The key difference in our approach is with the use of distributions to describe the fibril yield stretch and rupture stretch. Whilst modifying the fibril stress to become more flat can generate second linear regions, it is not enough to produce the range of behaviour observed by Goh et al. (2018). We must have a combination of both flattening fibril stress and a distribution of fibril yield stretch in order to capture all observed behaviour in region III. Without a distribution of yield stretch, the transition between a first and second linear region will be fixed by the fibril crimp distribution, meaning that sets of data with a narrow region I but a wide region III cannot be fitted using the model. Without a distribution of fibril rupture stretch, we cannot produce step-like failure behaviour at the tendon scale without also incorporating it at the fibril scale. Failure tests carried out on individual collagen fibrils show that this would not be realistic.

By using distributions to represent the failure properties of collagen fibrils, we are able to encapsulate the variation observed between the stress–strain curves of individual fibrils. There is not enough data available to study specific forms of these distributions, but we know that they will be heavily influenced by the structural properties of the fibrils. For example, changes in cross-link density synonymous with tendon maturation have been shown to alter the mechanical properties of fibrils, affecting the yield stretch in particular (Depalle et al., 2015). To model such a change using the framework introduced in this paper, we would simply feed this change into the yield stretch distribution, which would alter the whole tendon stress–strain curve.

Our model does not contain any direct dependence on collagen fibril diameter, but there is some evidence to suggest that step-like failure could be due to the tendon possessing a multimodal distribution of fibril diameters.Yamamoto and Nakamura (2017) were able to determine a relationship between collagen fibril diameter and failure strain, for fibrils extracted from mouse tail tendons. Fibrils with a larger diameter seemed to fail at larger strains. It could be the case that in stress–strain data where we see step-like failure behaviour, there is a multimodal distribution of collagen fibril diameters, leading to a multimodal distribution of fibril failure strain. Although it is common to see multimodal fibril diameter distributions in tendons (Chang et al., 2020), the diameter distributions recorded by Goh et al. (2018) seem to be unimodal for mice in the age groups where step-like failure is most commonly observed (see Table B.1 in Appendix B). Whilst this seems to contradict the theory that the step-like behaviour is due to groups of fibrils with different diameters failing in turn, it does not rule it out. The diameter distributions recorded by Goh et al. (2018) were found by taking the average across multiple fascicles, whilst the stress–strain data itself is from single fascicles. We cannot find the diameter distribution of a tendon and then stretch it to failure, as these are both destructive procedures. It remains plausible that the fascicles whose stress–strain curves contained step-like failure behaviour possess a multimodal diameter distribution, but that the average diameter distribution for that age group appears to be unimodal. Another possibility is that the relationship between collagen fibril diameter and rupture stretch is more complex than the linear relationship suggested by Yamamoto and Nakamura (2017), somehow causing the unimodal diameter distribution to result in a multimodal rupture stretch distribution. It could also be the case that it is the distribution of rupture stretch that gives rise to the distribution of diameters as the tendon matures, i.e. the fibrils may grow differently depending on their initial mechanical properties.

Using a multimodal distribution to represent the fibril failure strain is not the only way to account for the step-like failure behaviour observed at the macroscale. We can also produce this behaviour by having a multimodal distribution of critical stretch, representing a scenario where different fibre bundles have a different mean length. Step-like failure behaviour would therefore occur when these bundles fail at different times during a deformation. One attractive part of this approach is that it ties together the behaviour in every region of the tendon stress–strain curve, reducing the freedom brought about by the large number of parameters in the EPD model. However, if a tendon possesses a multimodal distribution of critical stretch, we would expect to see multiple distinct linear regions with increasing gradient before the tendon yields. We do not see this in any of the stress–strain data from Goh et al. (2018) where step-like failure is observed. It would still be possible to produce step-like failure behaviour with a single linear elastic region if there was a large amount of overlap between the yield stretch distribution and the additional modes of the critical stretch distribution. This would mean that fibrils in the first group begin to yield before fibrils in the other groups become taut, preventing additional linear regions and leading to steps in the macroscopic failure region. Fitting such a model to the data from Goh et al. would prove difficult in cases where all three distributions overlap due to the low number of data points in some of the tests.

Step-like failure could also be due to technical issues with the experiment, rather than due to the tissue microstructure itself. Clamping apparatus could cause fibre bundles to become differentially loaded, leading to some failing before others. Whilst this may have had an impact on the stress–strain data we were using, we chose to explore how this behaviour could arise from physiological differences in the tendon microstructure. In the absence of strong evidence for either the rupture stretch distribution or the critical stretch distribution being multimodal, we chose to do our fitting with the former for the sake of simplicity.

In order to get a sense of how our model compares with the ER model, we fitted both models to data from Goh et al. (2018). We chose to follow the physically motivated fitting approach for the EPD model, but opted to leave the lower bound of the yield stretch distribution a_Y as a fitting parameter, rather than setting it equal to the macroscopic yield point. Whilst this can lead to cases where some fibrils yield before others have become taut, the macroscopic yield data provided by Goh et al. proved to be too restrictive when used to fix the value of a_Y. To get a fair comparison between the EPD and ER models, we used symmetric triangular critical stretch distributions throughout, assuming that the lower bound of the critical stretch distribution a_C is equal to 1. This helped us to reduce the number of fitting parameters and lower the risk of overfitting. We found that in 82% of cases the EPD model provided a better fit than the ER model. In many of the remaining cases, the overall quality of the fit was hindered by a poor fit in the elastic region. This was often due to the assumption of symmetry in the critical stretch distribution, leading to an underestimation of the modulus, and a poor fit overall. The average RMSE reduced from 4.50 MPa using the ER model, to 2.29 MPa with the EPD model. The value of the plasticity parameter k found through fitting often did not change from its initial value of $k = 0$, suggesting that either it is not always that important to the model, or it cannot be determined from tendon stress–strain data alone.

It is difficult to judge whether the distributions used to generate the stress–strain curves in Figs. 9 and 10 are realistic because in all the references we could find, only a small number of collagen fibrils are stretched to failure. Liu et al. (2016) state that for fibrils extracted from rat patellar tendons, the yield point falls between 10% and 20% strain. In Fig. 9, the lower and upper bounds of the yield distribution are at 6% strain and 12% strain, respectively, whilst in Fig. 10, the yield distribution is bounded between 8% and 14% strain. The histograms of a_Y and b_Y presented in Fig. C.13 in Appendix C paint a similar picture: the mean values of a_Y and b_Y are 1.06 (6% strain) and 1.12 (12% strain), respectively. Despite the data from Goh et al. (2018) and Liu et al. (2016) coming from different sources, we believe that the similarities between the range of fibril yield strains observed experimentally, and the values we have found through our fitting, suggest that the EPD model is suitable for modelling the post-yield tendon behaviour (region III).

Fibrils tested by Liu et al. (2016) failed between 35% and 107% strain. Yamamoto et al. quote a failure strain of 34 ± 11% for fibrils extracted from mouse tail tendons (Yamamoto, 2017), and in a follow up paper, a range of 7%–81% (Yamamoto and Nakamura, 2017). All of these ranges exceed the upper bounds of the rupture distributions presented in Figs. 9 and 10, which are 23% and 25%, respectively. In fact, over all the fittings, the mean value of b_R was found to be 1.22 (22% strain). Liu et al. (2016) claim that because the tendon failure strain is typically much lower than the fibril rupture strain, there must be another component that is limiting the strength of the tendon, such as proteoglycans. We believe there are several reasons why the fibril rupture strain appears to be much larger than the tendon failure strain. Firstly, in tests carried out on individual collagen fibrils, the sections of fibril stretched to failure are much shorter than the entire length of the fibril. The fibrils tested by Yamamoto and Nakamura (2017) had a length of 19–64 μm, and whilst reliable data on the length of mouse tail tendon fibrils is not available, fibrils have been traced along the entire length (125 μm) of the mouse stapedius tendon (Svensson et al., 2017). If tail tendon fibrils are at least as long as those found in the stapedius tendon, then we can assume the sections tested by Yamamoto et al. were also significantly shorter than the total length of the fibril. Baldwin et al. (2020) provide evidence that collagen fibrils, extracted from bovine tail, possess regions of mechanical susceptibility, due to a variation in structure along the length of the fibril. If fibrils are continuous throughout the length of the tendon, then the strength of the tendon will be limited by the strength of the weakest parts of its fibrils. By only testing small sections of fibrils to failure, rather than entire fibrils, these weakest sections are likely to be missed. This would lead to an overestimation of the fibril strength, potentially having a large effect on the perceived failure strain of collagen fibrils, depending on the frequency and strength of the regions of mechanical susceptibility. This idea is supported by evidence from Svensson et al. (2018), who found that the failure strain of longer sections of fibril (>100 μm) extracted from rat tail tendons was around 9%, prompting them to come to similar conclusions. This is closer to the values we found through fitting, but still exceeded the failure strain of the whole tendon, which was found to be around 5%. Secondly, it is possible that fibrils are subjected to inhomogeneous strains within the tendon. This could be due to the geometry of the tendon, or because the mechanical properties of the fibrils vary through the length of the tendon. An inhomogeneous strain applied to a fibril could cause it to rupture at a lower value of end-to-end strain than it would otherwise rupture at, outside of the tendon. Although some of the fibril failure strains reported in the literature (Shen et al., 2010; Yamamoto and Nakamura, 2017) exceed the upper bounds of the rupture distributions used to generate the stress–strain curves in this paper, the quality of fit achieved demonstrates that the EPD model is still useful for modelling failure in tendons.

Throughout this paper we make a number of simplifying assumptions that may have a significant effect on its performance when it is used to model more complex deformations. We assume that fibrils are continuous and that damage on the macroscale occurs when the fibrils themselves become damaged. Whilst this approach is able to capture many of the stress–strain features observed experimentally, it may be necessary to extend the model to include interfibrillar sliding in order to fully capture all of the observed post-yield behaviour. There is some evidence that fibrils are discontinuous throughout the length of tendons (Peterson and Szczesny, 2020; Gupta et al., 2010; Puxkandl et al., 2002), and if the length of a fibril is shorter than some critical length (Agarwal et al., 2017), slippage between the fibril and the matrix will occur before the fibril itself can yield. Szczesny and Elliott (2014b,a) have shown that models based on this approach can be used to recreate the post-yield behaviour of tendons, getting good fits to experimental data. On the other hand, Craig et al. (1989) provide evidence that collagen fibrils in rat tail tendons are at least as long as the critical length required for fibrils to be structurally continuous.

The stress–strain curves of fibrils extracted from energy storing tendons have been shown to include an additional region of strain-stiffening, not present in the response of fibrils from positional tendons (Svensson et al., 2013; Quigley et al., 2018). The inclusion of interfibrillar sliding may be necessary in order to relate this behaviour to the macroscale tendon response. As imaging techniques improve and we get a better sense of the true length distribution of collagen fibrils, we will understand more about the mechanisms that lead to tendon failure. It may be possible in future to develop a failure model based on fibril length distribution, where fibrils below the critical length will slip, and those above the critical length will yield.

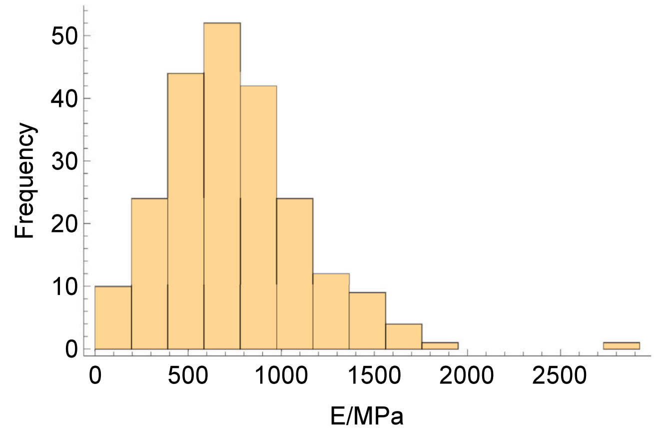

(a) Collagen fibril Young's modulus.

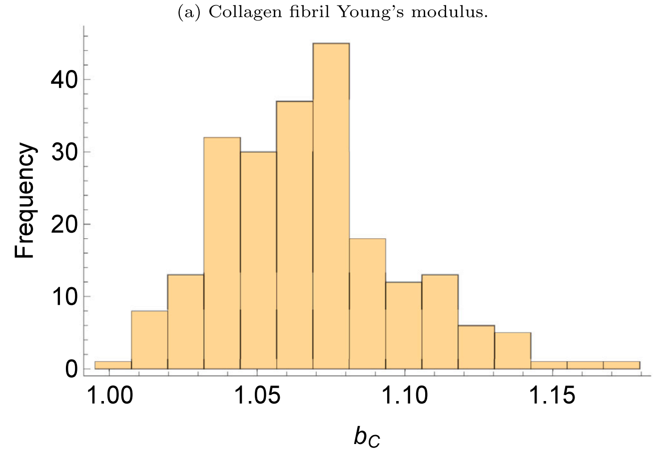

(b) Upper limit of the fibril critical stretch distribution.

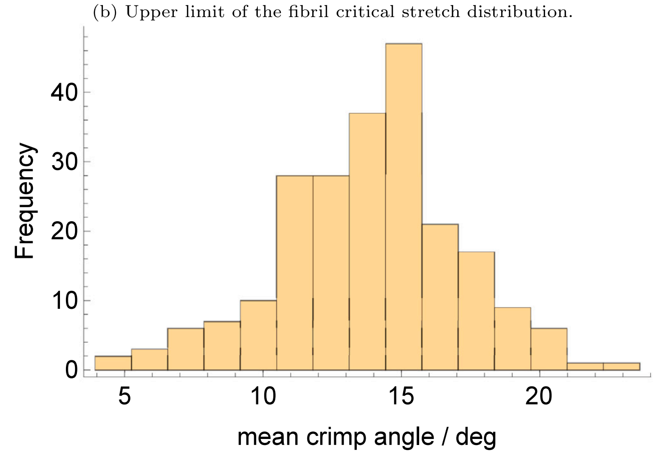

(c) Mean crimp angle found using equation (C.1).

Fig. C.13. Histograms of the EPD model parameters found by applying the fitting routine described in Section 4 to stress–strain data from Goh et al. (2018).

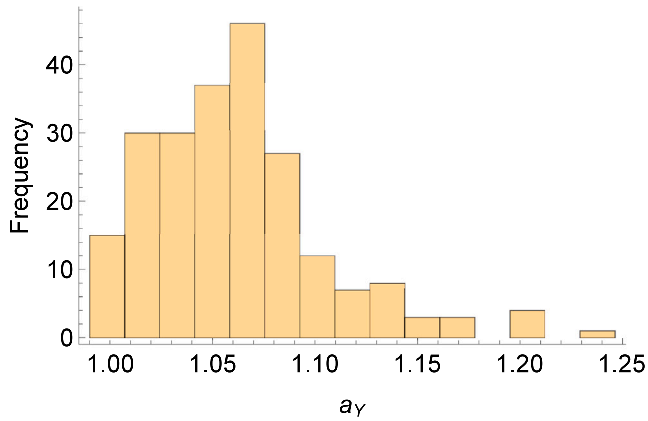

(d) Lower limit of fibril yield stretch distribution.

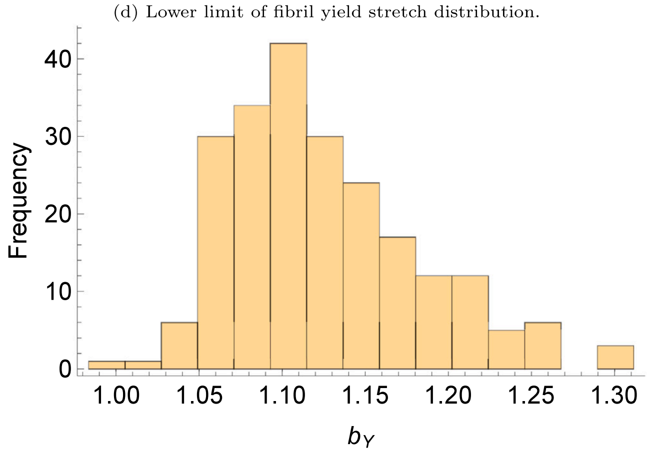

(e) Upper limit of the fibril yield stretch distribution.

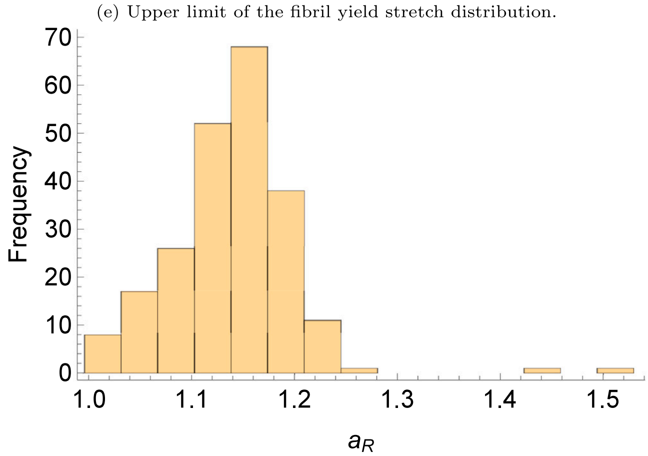

(f) Lower limit of the fibril rupture stretch distribution.

Fig. C.13. (*continued*).

There are several other simplifications we make that can be easily included when the model presented in this paper is used within a finite strain formulation. These include contributions to the stress from the extra-collagenous matrix, and the effects of fibre orientation. In the model presented by Hamedzadeh et al. (2018), the authors compute the stress in a way that allows them to incorporate a distribution of fibre orientation and a matrix term. A similar approach could be used to make our model more realistic, where the stress in the direction of the fibres is described using the expression in Eq. (5), with additional structural information imposed on top.

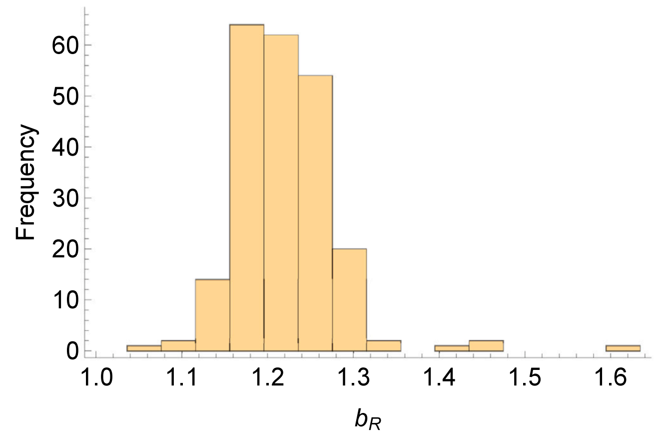

(g) Upper limit of the fibril rupture stretch distribution.

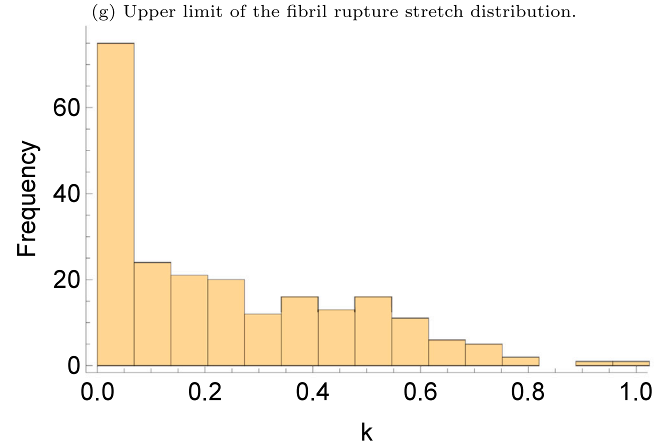

(h) The plasticity parameter k often did not change from its initial value of $k = 0$, which corresponds to the case of perfect plasticity.

Fig. C.13. (*continued*).

CRediT authorship contribution statement

James Gregory: Conceptualisation, Methodology, Writing - original draft. **Andrew L. Hazel:** Conceptualisation, Writing - review & editing. **Tom Shearer:** Conceptualisation, Writing - review & editing.

Declaration of competing interest

The authors declare that they have no known competing financial interests or personal relationships that could have appeared to influence the work reported in this paper.

Acknowledgement

Funding was provided by the UK Engineering and Physical Sciences Research Council (EPSRC) through the Doctoral Training Partnership (DTP) EP/R513131/1.

Appendix A. Analytic expression for the stress in the elastic-rupture model

When using the ER model, it is possible to determine an analytic expression for the stress in the tendon when the fibril critical stretch follows a triangular distribution. In this case, the tendon stress is given by

$$\sigma_T^{ER}(\lambda) = A^{ER} + B^{ER}\lambda + C^{ER}\lambda^2 + D^{ER}\lambda\log\lambda, \tag{A.1}$$

where A^{ER}, B^{ER}, C^{ER}, and D^{ER} are piecewise constants defined by

$$A^{ER} = \begin{cases} 0, & \lambda < a \quad \text{and} \quad \lambda/\lambda_R < a, \\ \dfrac{-a^2}{(a-b)(a-c)}, & a \le \lambda < c \quad \text{and} \quad \lambda/\lambda_R < a, \\ \dfrac{-bc}{(a-b)(b-c)} - \dfrac{a}{a-b}, & c \le \lambda < b \quad \text{and} \quad \lambda/\lambda_R < a, \\ -1, & \lambda \ge b \quad \text{and} \quad \lambda/\lambda_R < a, \\ 0, & a \le \lambda < c \quad \text{and} \quad a \le \lambda/\lambda_R < c, \\ \dfrac{c^2}{(a-c)(c-b)}, & c \le \lambda < b \quad \text{and} \quad a \le \lambda/\lambda_R < c, \\ \dfrac{b}{a-b} + \dfrac{ac}{(a-b)(a-c)}, & \lambda \ge b \quad \text{and} \quad a \le \lambda/\lambda_R < c, \\ 0, & c \le \lambda < b \quad \text{and} \quad c \le \lambda/\lambda_R < b, \\ \dfrac{b^2}{(a-b)(b-c)}, & \lambda \ge b \quad \text{and} \quad c \le \lambda/\lambda_R < b, \\ 0, & \lambda \ge b \quad \text{and} \quad \lambda/\lambda_R \ge b, \end{cases}$$

$$B^{ER} = \begin{cases} 0, & \lambda < a \quad \text{and} \quad \lambda/\lambda_R < a, \\ \dfrac{2a\log a}{(a-b)(a-c)}, & a \le \lambda < c \quad \text{and} \quad \lambda/\lambda_R < a, \\ \dfrac{2a\log a}{(a-b)(a-c)} + \dfrac{2c\log c}{(a-c)(b-c)}, & c \le \lambda < b \quad \text{and} \quad \lambda/\lambda_R < a, \\ \dfrac{2a\log a}{(a-b)(a-c)} - \dfrac{2b\log b}{(a-b)(b-c)} & \\ +\dfrac{2c\log c}{(a-c)(b-c)}, & \lambda \ge b \quad \text{and} \quad \lambda/\lambda_R < a, \\ \dfrac{2a[\lambda_R(1-\log\lambda_R)-1]}{\lambda_R(a-b)(a-c)}, & a \le \lambda < c \quad \text{and} \quad a \le \lambda/\lambda_R < c, \\ \dfrac{2c\log c}{(a-c)(b-c)} + \dfrac{2a[\lambda_R(1-\log\lambda_R)-1]}{\lambda_R(a-b)(a-c)}, & c \le \lambda < b \quad \text{and} \quad a \le \lambda/\lambda_R < c, \\ \dfrac{-2b\log b}{(a-b)(b-c)} + \dfrac{2c\log c}{(a-c)(b-c)} & \\ +\dfrac{2a[\lambda_R(1-\log\lambda_R)-1]}{\lambda_R(a-b)(a-c)}, & \lambda \ge b \quad \text{and} \quad a \le \lambda/\lambda_R < c, \\ \dfrac{2b[\lambda_R(1-\log\lambda_R)-1]}{\lambda_R(a-b)(b-c)}, & c \le \lambda < b \quad \text{and} \quad c \le \lambda/\lambda_R < b, \\ \dfrac{-2b\log b}{(a-b)(b-c)} + \dfrac{2b[\lambda_R(1-\log\lambda_R)-1]}{\lambda_R(a-b)(b-c)}, & \lambda \ge b \quad \text{and} \quad c \le \lambda/\lambda_R < b, \\ 0, & \lambda \ge b \quad \text{and} \quad \lambda/\lambda_R \ge b, \end{cases}$$

$$C^{ER} = \begin{cases} 0, & \lambda < a \quad \text{and} \quad \lambda/\lambda_R < a, \\ \dfrac{1}{(a-b)(a-c)}, & a \le \lambda < c \quad \text{and} \quad \lambda/\lambda_R < a, \\ \dfrac{1}{(a-b)(b-c)}, & c \le \lambda < b \quad \text{and} \quad \lambda/\lambda_R < a, \\ 0, & \lambda \ge b \quad \text{and} \quad \lambda/\lambda_R < a, \\ \dfrac{(\lambda_R-1)^2}{\lambda_R^2(a-b)(a-c)}, & a \le \lambda < c \quad \text{and} \quad a \le \lambda/\lambda_R < c, \\ \dfrac{1}{\lambda_R^2(a-b)(a-c)} + \dfrac{1}{(a-b)(b-c)} & \\ -\dfrac{2}{\lambda_R(a-b)(a-c)}, & c \le \lambda < b \quad \text{and} \quad a \le \lambda/\lambda_R < c, \\ \dfrac{(1-2\lambda_R)}{\lambda_R^2(a-b)(a-c)}, & \lambda \ge b \quad \text{and} \quad a \le \lambda/\lambda_R < c, \\ \dfrac{(\lambda_R-1)^2}{\lambda_R^2(a-b)(b-c)}, & c \le \lambda < b \quad \text{and} \quad c \le \lambda/\lambda_R < b, \\ \dfrac{(1-2\lambda_R)}{\lambda_R^2(a-b)(b-c)}, & \lambda \ge b \quad \text{and} \quad c \le \lambda/\lambda_R < b, \\ 0, & \lambda \ge b \quad \text{and} \quad \lambda/\lambda_R \ge b, \end{cases}$$

$$D^{ER} = \begin{cases} 0, & \lambda < a \quad \text{and} \quad \lambda/\lambda_R < a, \\ \dfrac{-2a}{(a-b)(a-c)}, & a \le \lambda < c \quad \text{and} \quad \lambda/\lambda_R < a, \\ \dfrac{-2b}{(a-b)(b-c)}, & c \le \lambda < b \quad \text{and} \quad \lambda/\lambda_R < a, \\ 0, & \lambda \ge b \quad \text{and} \quad \lambda/\lambda_R < a, \\ 0, & a \le \lambda < c \quad \text{and} \quad a \le \lambda/\lambda_R < c, \\ \dfrac{-2b}{(a-b)(b-c)} + \dfrac{2a}{(a-b)(a-c)}, & c \le \lambda < b \quad \text{and} \quad a \le \lambda/\lambda_R < c, \\ \dfrac{2a}{(a-b)(a-c)}, & \lambda \ge b \quad \text{and} \quad a \le \lambda/\lambda_R < c, \\ 0, & c \le \lambda < b \quad \text{and} \quad c \le \lambda/\lambda_R < b, \\ \dfrac{2b}{(a-b)(b-c)}, & \lambda \ge b \quad \text{and} \quad c \le \lambda/\lambda_R < b, \\ 0, & \lambda \ge b \quad \text{and} \quad \lambda/\lambda_R \ge b, \end{cases}$$

Appendix B. Age breakdown of features present in stress–strain data

Table B.1
The number of stress–strain curves from Goh et al. (2018) containing second linear regions N_{linear}, and step-like failure behaviour N_{steps} for each age group of mice, as described in Section 2.3. N_{either} gives the number with either a second linear region, step-like failure behaviour, or both. The final column gives the number with both N_{both}.

Age group	N_{total}	N_{linear}	N_{steps}	N_{either}	N_{both}
1.6 month	27	7 (26%)	16 (59%)	20 (74%)	3 (11%)
2.6 month	25	13 (52%)	14 (56%)	19 (76%)	8 (32%)
4.0 month	17	7 (41%)	7 (41%)	11 (65%)	3 (18%)
11.5 month	34	16 (47%)	3 (9%)	18 (53%)	1 (3%)
23.0 month	33	7 (21%)	3 (9%)	9 (27%)	1 (3%)
29.0 month	43	11 (26%)	4 (9%)	14 (33%)	1 (2%)
31.5 month	40	13 (33%)	3 (8%)	15 (38%)	1 (3%)
35.3 month	41	12 (29%)	4 (10%)	15 (37%)	1 (2%)
Total:	260	86 (33%)	54 (21%)	121 (47%)	19 (7%)

Appendix C. Fitting parameters

This section contains histograms showing the spread of the fitting parameters obtained when we fit the EPD model to 223 sets of stress–strain data from Goh et al. (2018). For a tendon with a distribution of critical stretch $\Lambda_C(\lambda_C)$, we can find the mean crimp angle θ by computing

$$\theta = \int_1^\infty \arccos\left(\frac{1}{\lambda_C}\right)\Lambda_C(\lambda_C)\,\mathrm{d}\lambda_C. \tag{C.1}$$

References

Agarwal, B.D., Broutman, L.J., Chandrashekhara, K., 2017. Analysis and Performance of Fiber Composites. John Wiley & Sons.

Alastrué, V., Rodríguez, J., Calvo, B., Doblaré, M., 2007. Structural damage models for fibrous biological soft tissues. Int. J. Solids Struct. 44 (18–19), 5894–5911.

Baldwin, S.J., Sampson, J., Peacock, C.J., Martin, M.L., Veres, S.P., Lee, J.M., Kreplak, L., 2020. A new longitudinal variation in the structure of collagen fibrils and its relationship to locations of mechanical damage susceptibility. J. Mech. Behav. Biomed. Mater. 103849.

Chang, J., Garva, R., Pickard, A., Yeung, C.-Y.C., Mallikarjun, V., Swift, J., Holmes, D.F., Calverley, B., Lu, Y., Adamson, A., et al., 2020. Circadian control of the secretory pathway maintains collagen homeostasis. Nature Cell Biol. 22 (1), 74–86.

Craig, A.S., Birtles, M.J., Conway, J.F., Parry, D.A., 1989. An estimate of the mean length of collagen fibrils in rat tail-tendon as a function of age. Connect. Tissue Res. 19 (1), 51–62.

Depalle, B., Qin, Z., Shefelbine, S.J., Buehler, M.J., 2015. Influence of cross-link structure, density and mechanical properties in the mesoscale deformation mechanisms of collagen fibrils. J. Mech. Behav. Biomed. Mater. 52, 1–13.

Goh, K.L., Holmes, D.F., Lu, Y.H., Kadler, K.E., Purslow, P.P., 2018. Age-related dataset on the mechanical properties and collagen fibril structure of tendons from a murine model. Sci. Data 5, 180140.

Grant, C.A., Brockwell, D.J., Radford, S.E., Thomson, N.H., 2008. Effects of hydration on the mechanical response of individual collagen fibrils. Appl. Phys. Lett. 92 (23), 233902.

Gupta, H., Seto, J., Krauss, S., Boesecke, P., Screen, H., 2010. In situ multi-level analysis of viscoelastic deformation mechanisms in tendon collagen. J. Struct. Biol. 169 (2), 183–191.

Hamedzadeh, A., Gasser, T.C., Federico, S., 2018. On the constitutive modelling of recruitment and damage of collagen fibres in soft biological tissues. Eur. J. Mech. A Solids 72, 483–496.

Hijazi, K.M., Singfield, K.L., Veres, S.P., 2019. Ultrastructural response of tendon to excessive level or duration of tensile load supports that collagen fibrils are mechanically continuous. J. Mech. Behav. Biomed. Mater. 97, 30–40.

Hurschler, C., Loitz-Ramage, B., Vanderby Jr, R., 1997. A structurally based stress-stretch relationship for tendon and ligament.

Lanir, Y., 1983. Constitutive equations for fibrous connective tissues. J. Biomech. 16 (1), 1–12.

Liu, Y., Ballarini, R., Eppell, S.J., 2016. Tension tests on mammalian collagen fibrils. Interface Focus 6 (1), 20150080.

Miyazaki, H., Hayashi, K., 1999. Tensile tests of collagen fibers obtained from the rabbit patellar tendon. Biomed. Microdevices 2 (2), 151–157.

Natali, A., Pavan, P., Carniel, E., Dorow, C., 2003. A transversally isotropic elasto-damage constitutive model for the periodontal ligament. Comput. Methods Biomech. Biomed. Eng. 6 (5–6), 329–336.

Natali, A., Pavan, P., Carniel, E., Lucisano, M., Taglialavoro, G., 2005. Anisotropic elasto-damage constitutive model for the biomechanical analysis of tendons. Med. Eng. Phys. 27 (3), 209–214.

Peterson, B.E., Szczesny, S.E., 2020. Dependence of tendon multiscale mechanics on sample gauge length is consistent with discontinuous collagen fibrils. Acta Biomater. 117, 302–309.

Puxkandl, R., Zizak, I., Paris, O., Keckes, J., Tesch, W., Bernstorff, S., Purslow, P., Fratzl, P., 2002. Viscoelastic properties of collagen: synchrotron radiation investigations and structural model. Philos. Trans. R. Soc. Lond. Ser. B: Biol. Sci. 357 (1418), 191–197.

Quigley, A.S., Bancelin, S., Deska-Gauthier, D., Légaré, F., Kreplak, L., Veres, S.P., 2018. In tendons, differing physiological requirements lead to functionally distinct nanostructures. Sci. Rep. 8 (1), 1–14.

Rodríguez, J.F., Cacho, F., Bea, J.A., Doblaré, M., 2006. A stochastic-structurally based three dimensional finite-strain damage model for fibrous soft tissue. J. Mech. Phys. Solids 54 (4), 864–886.

Shearer, T., 2015a. A new strain energy function for modelling ligaments and tendons whose fascicles have a helical arrangement of fibrils. J. Biomech. 48 (12), 3017–3025.

Shearer, T., 2015b. A new strain energy function for the hyperelastic modelling of ligaments and tendons based on fascicle microstructure. J. Biomech. 48 (2), 290–297.

Shearer, T., Parnell, W.J., Lynch, B., Screen, H.R., David Abrahams, I., 2020. A recruitment model of tendon viscoelasticity that incorporates fibril creep and explains strain-dependent relaxation. J. Biomech. Eng. 142 (7).

Shearer, T., Thorpe, C.T., Screen, H.R., 2017. The relative compliance of energy-storing tendons may be due to the helical fibril arrangement of their fascicles. J. R. Soc. Interface 14 (133), 20170261.

Shen, Z.L., Dodge, M.R., Kahn, H., Ballarini, R., Eppell, S.J., 2008. Stress-strain experiments on individual collagen fibrils. Biophys. J. 95 (8), 3956–3963.

Shen, Z.L., Dodge, M.R., Kahn, H., Ballarini, R., Eppell, S.J., 2010. In vitro fracture testing of submicron diameter collagen fibril specimens. Biophys. J. 99 (6), 1986–1995.

Sun, M., Connizzo, B.K., Adams, S.M., Freedman, B.R., Wenstrup, R.J., Soslowsky, L.J., Birk, D.E., 2015. Targeted deletion of collagen v in tendons and ligaments results in a classic ehlers-danlos syndrome joint phenotype. Amer. J. Pathol. 185 (5), 1436–1447.

Svensson, R.B., Herchenhan, A., Starborg, T., Larsen, M., Kadler, K.E., Qvortrup, K., Magnusson, S.P., 2017. Evidence of structurally continuous collagen fibrils in tendons. Acta Biomater. 50, 293–301.

Svensson, R.B., Mulder, H., Kovanen, V., Magnusson, S.P., 2013. Fracture mechanics of collagen fibrils: influence of natural cross-links. Biophys. J. 104 (11), 2476–2484.

Svensson, R.B., Smith, S.T., Moyer, P.J., Magnusson, S.P., 2018. Effects of maturation and advanced glycation on tensile mechanics of collagen fibrils from rat tail and achilles tendons. Acta Biomater. 70, 270–280.

Szczesny, S.E., Elliott, D.M., 2014a. Incorporating plasticity of the interfibrillar matrix in shear lag models is necessary to replicate the multiscale mechanics of tendon fascicles. J. Mech. Behav. Biomed. Mater. 40, 325–338.

Szczesny, S.E., Elliott, D.M., 2014b. Interfibrillar shear stress is the loading mechanism of collagen fibrils in tendon. Acta Biomater. 10 (6), 2582–2590.

Van Der Rijt, J.A., Van Der Werf, K.O., Bennink, M.L., Dijkstra, P.J., Feijen, J., 2006. Micromechanical testing of individual collagen fibrils. Macromol. Biosci. 6 (9), 697–702.

Yamamoto, N., 2017. Tensile strength of single collagen fibrils isolated from tendons. Eur. J. Biophys. 5 (1), 1.

Yamamoto, N., Nakamura, S., 2017. Relationships between the tensile strength and diameter of collagen fibrils isolated from mouse tail tendons. J. Biomech. Sci. Eng. 12 (3), 16–00511.

Zitnay, J.L., Li, Y., Qin, Z., San, B.H., Depalle, B., Reese, S.P., Buehler, M.J., Yu, S.M., Weiss, J.A., 2017. Molecular level detection and localization of mechanical damage in collagen enabled by collagen hybridizing peptides. Nature Commun. 8 (1), 1–12.